AMERICAN SOCIETY FOR MICROBIOLOGY | Applied and Environmental Microbiology®

ENVIRONMENTAL MICROBIOLOGY

Multi-Omics Profiling Reveals Resource Allocation and Acclimation Strategies to Temperature Changes in a Marine Dinoflagellate

Hao Zhang,[a] Bowei Gu,[a] Youping Zhou,[b,f,g] Xiao Ma,[a] Tianqi Liu,[c] Hongkai Xu,[d] Zhangxian Xie,[c] Kailin Liu,[e] Dazhi Wang,[c] Xiaomin Xia[a,h]

[a]CAS Key Laboratory of Tropical Marine Bio-Resources and Ecology, South China Sea Institute of Oceanology, Chinese Academy of Sciences, Guangzhou, China
[b]Department of Ocean Science and Engineering, Southern University of Science and Technology (SUSTech), Shenzhen, China
[c]State Key Laboratory of Marine Environmental Science/College of the Environment and Ecology, Xiamen University, Xiamen, China
[d]BGI-Shenzhen, Shenzhen, China
[e]Department of Mathematics and Statistics, University of Strathclyde, Glasgow, United Kingdom
[f]Isotopoimics in Chemical Biology (ICB), School of Chemistry and Chemical Engineering, Shaanxi University of Science and Technology, Xi'an, China
[g]Southern Marine Science and Engineering Guangdong Laboratory (Zhuhai), Zhuhai, China
[h]Southern Marine Science and Engineering Guangdong Laboratory (Guangzhou), Guangzhou, China

ABSTRACT Temperature is a critical environmental factor that affects the cell growth of dinoflagellates and bloom formation. To date, the molecular mechanisms underlying the physiological responses to temperature variations are poorly understood. Here, we applied quantitative proteomic and untargeted metabolomic approaches to investigate protein and metabolite expression profiles of a bloom-forming dinoflagellate *Prorocentrum shikokuense* at different temperatures. Of the four temperatures (19, 22, 25, and 28°C) investigated, *P. shikokuense* at 25°C exhibited the maximal cell growth rate and maximum quantum efficiency of photosystem II (Fv/Fm) value. The levels of particulate organic carbon (POC) and nitrogen (PON) decreased with increasing temperature, while the POC/PON ratio increased and peaked at 25°C. Proteomic analysis showed proteins related to photoreaction, light harvesting, and protein homeostasis were highly expressed at 28°C when cells were under moderate heat stress. Metabolomic analysis further confirmed reallocated amino acids and soluble sugars at this temperature. Both omic analyses showed glutathione metabolism that scavenges the excess reactive oxygen species, and transcription and lipid biosynthesis that compensate for the low translation efficiency and plasma membrane fluidity were largely upregulated at suboptimal temperature. Higher accumulations of glutathione, glutarate semialdehyde, and 5-KETE at 19°C implied their important roles in low-temperature acclimation. The strikingly active nitrate reduction and nitrogen flux into asparagine, glutamine, and aspartic acid at 19°C indicated these three amino acids may serve as nitrogen storage pools and help cells cope with low temperature. Our study provides insights into the effects of temperature on dinoflagellate resource allocation and advances our knowledge of dinoflagellate bloom formation in marine environments.

IMPORTANCE Marine phytoplankton is one of the most important nodes in global biogeochemical cycle. Deciphering temperature-associated marine phytoplankton cell stoichiometric changes and the underlying molecular mechanisms are therefore of great ecological concerns. However, knowledge of how phytoplankton adjust the cell stoichiometry to sustain growth under temperature changes is still lacking. This study investigates the variations of protein and metabolite profiles in a marine dinoflagellate across temperatures at which the field blooms usually occur and highlights the temperature-dependent molecular traits and key metabolites that may be associated with rapid cell growth and temperature stress acclimation.

Editor Laura Villanueva, Royal Netherlands Institute for Sea Research

Address correspondence to Hao Zhang, zhanghao@scsio.ac.cn, or Xiaomin Xia, xiaxiaomin@scsio.ac.cn.

The authors declare no conflict of interest.

Received 19 July 2022
Accepted 26 July 2022
Published 17 August 2022

KEYWORDS temperature, dinoflagellate, harmful algal blooms, quantitative proteomics, metabolomics, phytoplankton stoichiometry

Among the biotic and abiotic parameters, temperature is recognized as a significant factor modulating the diversity and distribution of phytoplankton in global oceans (1, 2). It affects phytoplankton abundance directly through its effect on the rates of cell metabolism and cell division and indirectly through its effect on ocean stratification, which influences the movement of bottom level nutrients to surface oligotrophic seawater (3, 4). Dinoflagellates are one widespread and abundant phytoplankton group in global oceans. They are the major source of harmful algal blooms (HABs), which can severely affect marine ecosystems and aquaculture (5, 6). Long-term field investigation and niche model analyses show that the coastal dinoflagellate blooms are increasing due to ocean warming, in terms of frequency, intensity, and geographic distribution (7, 8). Since the phylogenetically diverse dinoflagellates exhibit distinct thermal traits (9), understanding the functional response to temperature among different species is therefore a requisite for the prediction and management of dinoflagellate blooms.

The phytoplankton growth-temperature relationship often exhibits a bell-shaped curve with gradual increases and steep declines in growth rate at sub- and supraoptimal temperatures (10). Each species is known to exhibit a narrow range of temperature for optimal cell growth (11, 12). Outside the optimal temperature range, cell motility, biochemical properties, and stoichiometry will vary largely. Dinoflagellates and other phytoplankton have adopted a series of response strategies to cope with sub- and supraoptimal temperatures, such as regulating nutrient acquisition, reallocating element stoichiometry, biosynthesizing protective compatible solutes and antioxidant metabolites, and changing the fluxes of vital metabolic pathways (13–15). In addition, high levels of photoprotective pigments at supraoptimal temperature and accumulations of polyunsaturated fatty acids and toxins at suboptimal temperature have been reported in dinoflagellates (16–19). All these strategies are aimed at establishing a new balance of resource allocation and energy consumption that will enable cells to survive and reproduce at nonoptimal temperatures.

Thus, deciphering temperature acclimation-related molecular events in phytoplankton is important for predicting the community variations under climate change and identifying traits that are subject to environmental selection. Using metatranscriptomics, Toseland et al. (20) found that phytoplankton significantly increase the rate of protein synthesis and decrease the number of ribosomes and their associated rRNAs as temperature rises. Increasing photosynthetic electron transport at low temperature and upregulating oxidative phosphorylation at high temperature are invoked to compensate for repressed photosynthesis in a green alga (21). Pathways to maintain necessary protein processing machinery and membrane structure are induced at nonoptimal temperatures in diatoms (22). To date, only several temperature stress-related genes/proteins are established in dinoflagellates (23, 24), and responses of a global metabolism to temperature changes in this phytoplankton group using multi-omics approaches are still less studied.

The dinoflagellate *Prorocentrum shikokuense* annually forms extensive large-scale HABs in the coastal East China Sea (ECS) in the spring (25, 26). Field investigations show that *P. shikokuense* exhibits relatively high growth rates between 16°C and 26°C in the coastal ECS (27). In the laboratory, it is able to grow at temperatures ranging from 10°C to 31°C (28). In our study, culture temperatures of 19, 22, 25, and 28°C were used to simulate temperature transitions from the early to late spring in the coastal ECS, covering the temperature range of a whole bloom period. The goal of this study was to decipher the underlying traits associated with temperature responses that may facilitate *P. shikokuense* to form blooms in spring. The iTRAQ-based quantitative proteomics and untargeted metabolomics approaches were used to investigate the protein and metabolite profiles of *P. shikokuense*. Our results showed some proteins and macromolecules that may serve as important agents of stress response and nutrient storage to sustain cell growth under different temperatures.

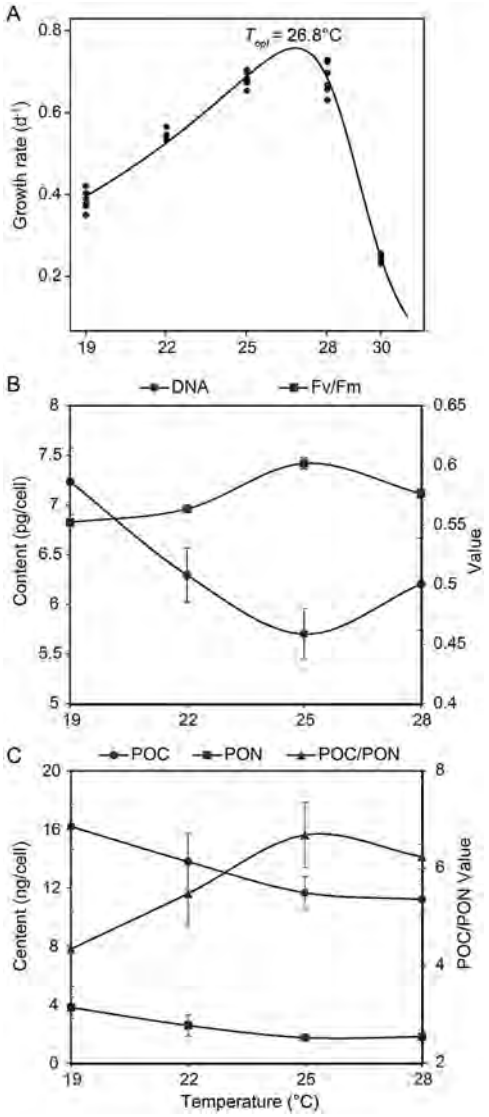

FIG 1 The physiological responses of *Prorocentrum shikokuense* at different temperatures. Growth rate (A), Fv/Fm value and DNA content (B), POC and PON content, and POC/PON ratio (C). POC: particulate organic carbon, PON: particulate organic nitrogen.

RESULTS

Physiological parameters at different temperatures. The growth rates of *P. shikokuense* at 19, 22, 25, and 28°C were 0.39, 0.54, 0.68, and 0.69 d^{-1}, respectively. Significant differences in the growth rates were observed between any pair of the four temperatures except 25°C and 28°C ($P < 0.05$). The optimal temperature of *P. shikokuense* was determined to be 26.8°C through Boltzmann-Arrhenius model analysis (Fig. 1A). Maximum quantum efficiency of photosystem II (Fv/Fm) values and DNA contents at 19, 22, 25, and 28°C were 0.55, 0.56, 0.60, and 0.58, and 7.24, 6.30, 5.71, and 6.21 pg/cell, respectively (Fig. 1B).

The POC and PON decreased with increasing temperatures, but the ratios of POC/PON increased from 19°C to 25°C and then decreased at 28°C (Fig. 1C). The POC and PON for 19, 22, 25, and 28°C were 16.18, 13.79, 11.66, and 11.21 ng/cell and 3.80, 2.57, 1.75, and 1.80 ng/cell, while the ratios of POC/PON were 4.34, 5.48, 6.68, and 6.24, respectively.

Overview of the quantitative iTRAQ proteomics. In total, 70,898 of the output 336,029 mass spectra matched 22,308 peptides, which resulted in the identification of 4,562 high-confidence proteins. Of the high-confidence proteins, 3,933 (86.3%) and

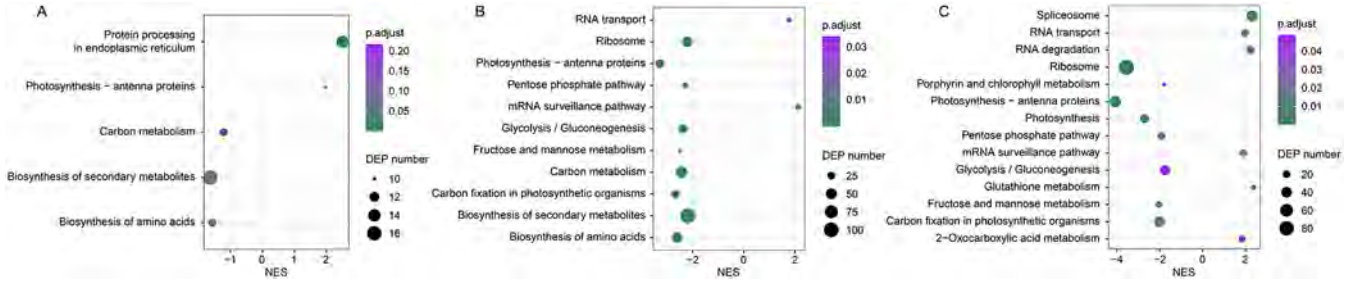

FIG 2 KEGG enrichment of differentially expressed proteins (DEPs) at 28°C versus 25°C (A), 22°C versus 25°C (B), and 19°C versus 25°C (C). Functional categories of DEPs are grouped at KEGG level 3. GSEA-derived normalized enrichment scores (NES) for DEPs are shown. A positive NES of 22°C versus 25°C indicates that the pathway was highly enriched at 22°C, while a negative NES of 22°C versus 25°C indicates that the pathway was highly enriched at 25°C. *P* adjusted <0.05 indicates a significant enrichment.

3,044 (66.8%) proteins were annotated using the NCBI nonredundant protein (NCBInr) and Kyoto Encyclopedia of Genes and Genomes (KEGG) databases, respectively. Compared with 25°C, 375, 1,274, and 1,918 differentially expressed proteins (DEPs) were identified at 28, 22, and 19°C, respectively (Fig. S1A). Heatmap based on protein expressions revealed that DEPs at 19°C and 22°C and at 25°C and 28°C were clustered together with high similarities, respectively (Fig. S2A). Moreover, most DEPs showed clear patterns of increase or decrease from 19°C to 28°C (Fig. S2B).

KEGG pathway enrichment analysis showed that the pathways related to protein processing in the endoplasmic reticulum and photosynthesis-antenna proteins were significantly enriched at 28°C relative to 25°C, whereas carbon metabolism and biosynthesis of secondary metabolites and amino acids were highly but not significantly enriched at 25°C relative to 28°C (Fig. 2A). A comparison between 22°C and 25°C showed that the mRNA surveillance pathway and RNA transport were significantly enriched at 22°C, while ribosome, carbon metabolism, carbon fixation, glycolysis/gluconeogenesis, fructose and mannose metabolism, pentose phosphate pathway, biosynthesis of amino acids and secondary metabolites, and photosynthesis-antenna proteins were significantly enriched at 25°C (Fig. 2B). A comparison between 19°C and 25°C showed that the spliceosome, mRNA surveillance pathway, RNA transport and degradation, 2-oxocarboxylic acid metabolism, and glutathione metabolism were significantly enriched at 19°C, while ribosome, carbon fixation, glycolysis/gluconeogenesis, fructose and mannose metabolism, pentose phosphate pathway, porphyrin and chlorophyll metabolism, photosynthesis, and photosynthesis-antenna proteins were significantly enriched at 25°C (Fig. 2C).

Overview of the untargeted metabolomics. We detected a total of 331 metabolites from cells growing at 19, 25, and 28°C. Among them, 142 and 116 differentially expressed metabolites (DEMs) were identified at 28°C versus 25°C and 19°C versus 25°C, respectively (Fig. S1B). Most of these DEMs were identified and classified as amino acids, peptides and their analogues, carbohydrates and carbohydrate conjugates, and fatty acids and conjugates. More upregulated DEMs belonging to purine and pyridine nucleosides, fatty acids and conjugates, amino acids, peptides and analogues, benzene and substituted derivatives, and carbohydrates and carbohydrate conjugates were observed at 28°C compared with 25°C (Fig. 3A), while more upregulated DEMs belonging to purine and pyridine nucleosides were observed at 19°C compared with 25°C (Fig. 3B).

Compared with 25°C, metabolisms of amino sugar and nucleotide sugar, arginine and proline, fructose and mannose, galactose, glyoxylate and dicarboxylate, nicotinate and nicotinamide, and isoquinoline alkaloid biosynthesis with more DEMs were enriched at 28°C (Fig. 4A). A comparison between 19°C and 25°C showed that metabolisms of glutathione, purine, arachidonic acid, beta-alanine, cysteine, and methionine with more DEMs were enriched at 19°C, while galactose metabolism and carbapenem biosynthesis with more DEMs were enriched at 25°C (Fig. 4B).

Cell growth-related and stress response-related DEPs and DEMs between 28°C and 25°C. For proteomics, DEPs involved in photosynthesis, and photosynthesis-antenna proteins, such as chlorophyll a-c binding protein (CAB), light harvesting protein (LHP), PsaB,

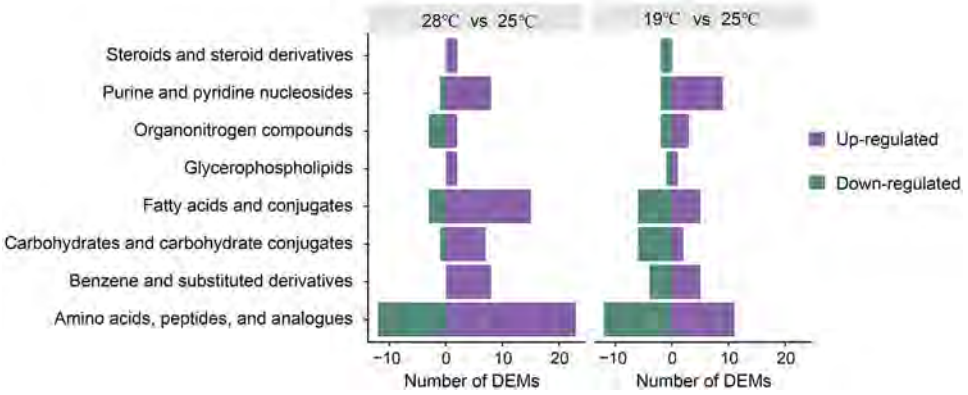

FIG 3 Classification and distribution of differentially expressed metabolites (DEMs) between temperature comparisons. "28°C versus 25°C" means 28°C compared with 25°C.

and PsaC were significantly upregulated at 28°C relative to 25°C (Fig. 5A). Moreover, heat shock protein 90 (HSP90) was also upregulated at 28°C. The majority of DEPs involved in carbohydrate metabolism, translation, and amino acid metabolism were upregulated at 25°C relative to 28°C. For metabolomics, abundances of carbohydrates and amino acids varied largely between 25°C and 28°C (Fig. 5B). The typical carbohydrates L-fucose, mannitol, and D-mannose and amino acids L-proline and L-lysine were largely accumulated at 28°C, while amino acids L-asparagine, L-histidine, ornithine, and L-glutamine were largely accumulated at 25°C.

Cell growth-related and stress response-related DEPs and DEMs across 19°C, 22°C, and 25°C. Cell growth-related proteins such as carbonic anhydrate (CA), ribulose 1,5-bisphosphate carboxylase/oxygenase (RBC), nitrate transporter (NT), LHP, and CAB were significantly downregulated at 19°C and 22°C relative to 25°C, while those involved in stress responses such as copper/zinc superoxide dismutase (Cu/Zn SOD) were significantly upregulated at both 19°C and 22°C (Fig. 6A and B). Specifically, more DEPs involved in cold acclimation and lipid and nucleotide metabolisms, such as cold shock protein (CSP), long-chain fatty acid CoA ligase (ACSBG), acetyl-CoA acyltransferase 1 (ACAA1), long-chain acyl-CoA synthetase (ACSL), uridine kinase (udk), CTP synthase (pyrG), GMP synthase (guaA), IMP dehydrogenase (IMPDH), and adenosine kinase (ADK), were significantly upregulated at 19°C relative to 25°C (Fig. 6B, Fig. S3, and Table S1).

A comparison between 19°C and 25°C showed that amino acids gamma-aminobutyric acid (GABA), L-glutamine, L-aspartic acid, and L-asparagine were accumulated at 19°C, while L-lysine and L-proline were accumulated at 25°C (Fig. 6C). Fatty acids gluta-

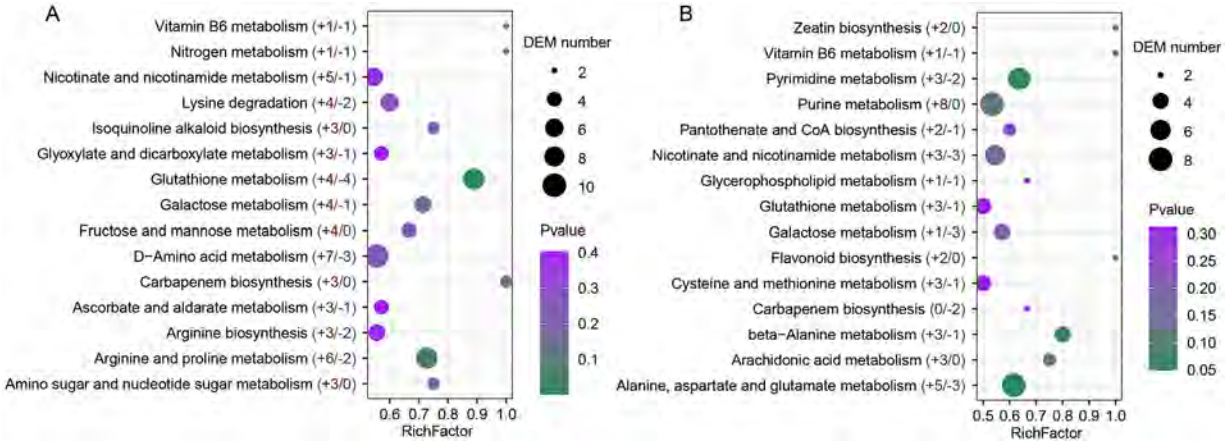

FIG 4 The top 15 enriched KEGG terms of differentially expressed metabolites (DEMs) at 28°C versus 25°C (A) and 19°C versus 25°C (B). Red numbers with plus signs and blue numbers with minus signs indicate upregulated and downregulated DEMs, respectively.

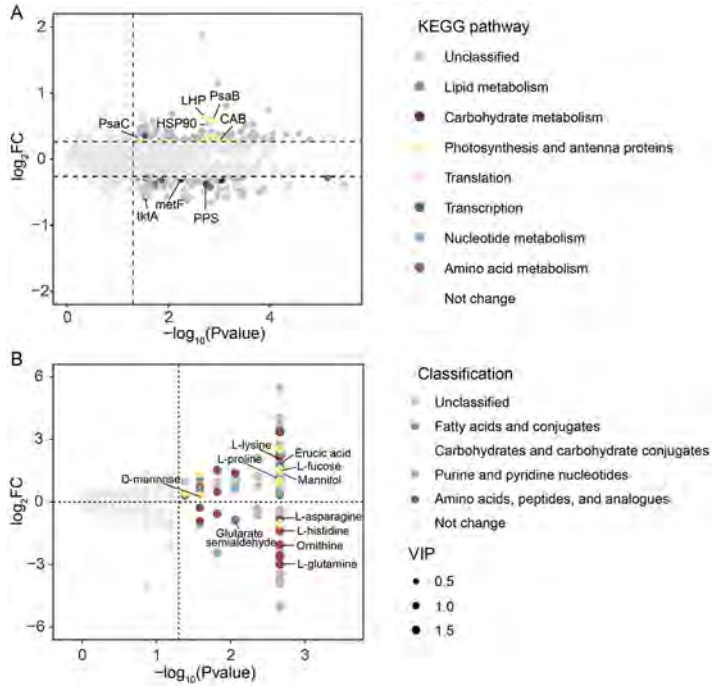

FIG 5 Color-coded scatterplots of $\log_2$ fold change in protein (A) and metabolite (B) abundances at 28°C versus 25°C. "28°C versus 25°C" means 28°C compared with 25°C. Functional categories of differentially expressed proteins (DEPs) are grouped at the KEGG level 2.

rate semialdehyde and 5-KETE were accumulated at 19°C, indicating their important roles at low temperature acclimation. Unlike other metabolites, the majority of the differentially expressed purine and pyridine nucleotides, such as IMP, AMP, thiamine, cytosine, inosine, adenosine, and adenine, were observed to have accumulated at 19°C (Fig. 6C and Fig. S4D).

DISCUSSION

Changes in essential resource allocation associated with rapid cell growth when temperature increased from 19°C to 25°C. Temperature is recognized as one of the most important drivers affecting cell growth and the stoichiometry of phytoplankton in global oceans (20). In our study, cell growth rates of *P. shikokuense* gradually increased from 19°C to 25°C (Fig. 1A), accompanied by the increased numbers of upregulated DEPs involved in photosynthesis-antenna proteins, photosynthesis, translation, carbon fixation, glycolysis/gluconeogenesis, fructose and mannose metabolism, and pentose phosphate pathway (Fig. 2 and Table S1). Among these pathways, abundances of the indicative proteins, such as LHPs, photosystem genes, NT, CA, RBC, and ribosomal proteins, increased from 19°C to 25°C (Fig. 6A and B and Table S1). These results suggested that *P. shikokuense* actively incorporated and allocated light, CO_2, and nutrients into the necessary macromolecules of carbohydrates, chlorophylls (Chls), and proteins essential for cell division to support rapid cell growth at high temperature. Consistent with the proteomics screening, the majority of identified DEMs belonging to carbohydrates and fatty acids were found to accumulate with increasing temperatures (Fig. 3).

Cell stoichiometry is the result of cellular resource allocation across different compound classes that vary in their carbon (C), nitrogen (N), and phosphate (P) contents. Generally, the major constituents of polysaccharides, lipids and carbohydrates, Chls, amino acids and proteins, and DNA and RNA are C, N, and P, respectively (29). The proteomics and metabolomics results showed that C was mainly allocated to carbohydrates, while N was largely allocated to Chls and proteins with increasing temperatures. Healthy cultures of phytoplankton usually exhibit a Redfield C:N ratio around 106:16 (6.63) (30). To date, the global data still show no repeatable relationship between temperature and phytoplankton C:N

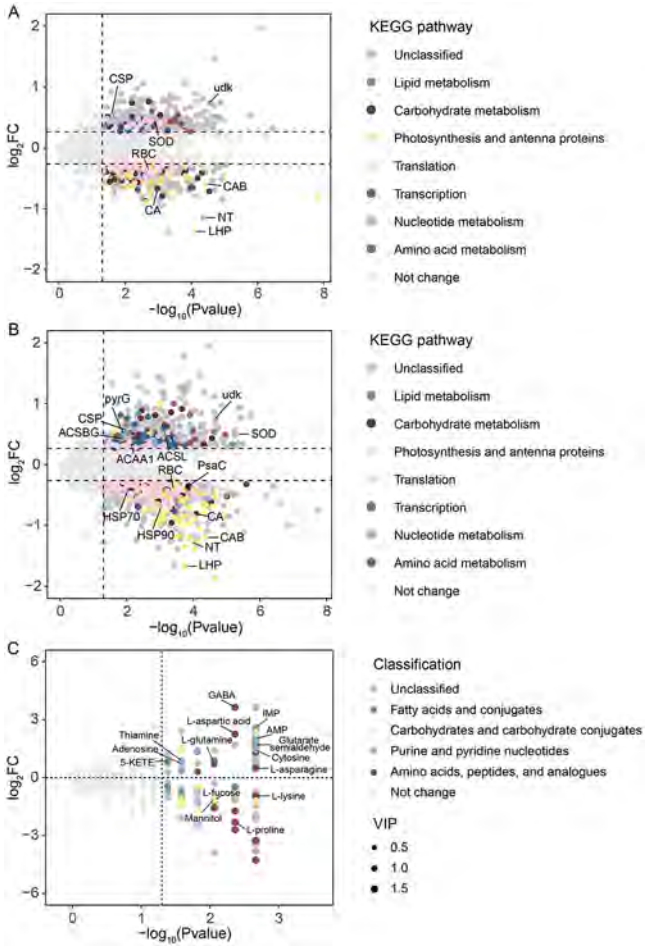

FIG 6 Color-coded scatterplots of $\log_2$ fold change in protein abundance at 22°C versus 25°C (A), and 19°C versus 25°C (B), and $\log_2$ fold change in metabolite abundance at 19°C versus 25°C (C). "22°C versus 25°C" means 22°C compared with 25°C. Functional categories of differentially expressed proteins (DEPs) are grouped at the KEGG level 2.

ratios (31, 32). For *P. shikokuense*, the contents of POC and PON per cell decreased from 19°C to 25°C (Fig. 1C). This can be explained by the "temperature-size rule" in phytoplankton that cell body size decreases when temperature increases (31, 33). Meanwhile, the POC/PON ratio of *P. shikokuense* increased and peaked at 25°C with a value of 6.68 (very close to 106:16). This change in POC/PON ratio may be due to the fact that the PON content decreased faster than POC when exposed to higher temperature and is consistent with the finding of a previous study that diatom cells with smaller size at high temperature may increase photosynthetic efficiency per Chl *a* and boost cellular C per biovolume with low N input (34). Among the detected carbohydrates, L-fucose and mannitol varied largely and accumulated gradually with increasing temperatures (Fig. 6C and Fig. S4B). L-fucose, a common monosaccharide produced by algae, is a major component of fucose-containing sulfated polysaccharides (FCSPs). The recalcitrant FCSPs are known to resist microbial enzymatic degradation and contribute largely to marine C sinks after the diatom blooms (35). On the other hand, mannitol is one of the major photosynthetic products that serve as important C storage and antioxidant in algae (36). Field studies showed significant increases in mannitol in some algae during summer compared with other seasons (37). Taken together, these results suggested that warming may enhance the accumulations of L-fucose and mannitol in marine phytoplankton.

Acclimation strategies in response to supraoptimal temperature. The Fv/Fm value is a measure of the maximum quantum efficiency of photosystem II (PSII) and is widely used as a stress indicator in phytoplankton studies (38). We observed that *P.*

shikokuense had a similar growth rate but significantly lower Fv/Fm value at 28°C than 25°C (Fig. 1B), suggesting the supraoptimal temperature of 28°C had affected the algal biophysiological activities. Photosystems are particularly sensitive to thermal stress in photosynthetic organisms (39). DEPs in *P. shikokuense* involved in photosynthesis and photosynthesis-antenna proteins were more abundant at 28°C than 25°C (Fig. 5A). Among them, higher expressions of psaB and psaC, which are the essential enzymes for the catalysis of light-induced water oxidation and electron transfer across thylakoid membrane, reinforced photoreaction of *P. shikokuense* to compensate for the reduced quantum efficiency of PSII under thermal stress. Moreover, we observed concomitant increased expression levels of several CABs and LHPs at 28°C (Fig. 5A and Table S1). CABs are one vital component of light harvesting complex (40). In addition to acting as light harvesting agents in dinoflagellates, CABs and LHPs can prevent thermal stress-induced photo-damage in cells through dissipating the excessive heat and protecting the photosynthetic apparatus (41, 42).

HSPs act as molecular chaperones by preventing the aggregation of misfolded proteins at high temperatures (43, 44). Accumulation of HSPs in various organisms under thermal stress has been widely observed, including the temperate, tropical, and symbiotic dinoflagellates (23, 24, 45). In addition, HSP70 plays an essential role in repairing the disassembled PSII core complex through binding to the thylakoid membrane in green algae (46). Higher expression of HSP70 and HSP90 at 28°C may protect the protein structure and ensure PSII stability in *P. shikokuense* (Fig. 5A, Fig. S3A, and Table S1). Also, even moderate thermal stress can disrupt cellular protein homeostasis and reallocation of amino acids, which was evidenced by the boosted protein processing in the endoplasmic reticulum, and a large number of differentially expressed amino acids between 28°C and 25°C (Fig. 2A and 3). Among these amino acids, proline was found to be related to a variety of thermal resistance in numerous plants (47). The finding that higher content of L-proline in *P. shikokuense* at 28°C (than 25°C) (Fig. 5B) implies that L-proline is a key amino acid in thermal protection.

Carbon metabolism in *P. shikokuense* was negatively affected by the moderate thermal stress at 28°C compared with 25°C (Fig. 2A). Thermal stress normally modifies carbon metabolism through inhibiting enzyme activities and downregulating genes expressions (48). In our study, carbon metabolism related-enzymes of pyruvate water dikinase (PPS), transketolase (tktA), methylenetetrahydrofolate reductase (metF), and glycine hydroxymethyltransferase (SHMT) were significantly downregulated at 28°C than 25°C (Table S1). The downregulated carbon metabolism will reallocate organic carbohydrates between polysaccharides and soluble sugars. Since heat stress interrupts intracellular osmotic homeostasis, accumulations of soluble sugars to reduce the negative effects has been observed in plants (49). The enriched mechanisms of fructose and mannose and galactose in *P. shikokuense* at 28°C suggested their important roles at heat stress acclimation (Fig. 4A). Thus, the significantly accumulated monosaccharides of L-fucose, mannitol, D-mannose, sorbitol, and stachyose that involved in these two processes may function at osmotic adjustment under the moderate thermal stress (Fig. S4B and Table S2).

Acclimation strategies in response to suboptimal temperature. Compared with 25°C, the suboptimal temperatures of 19°C and 22°C seriously influenced the cell growth and photosystem of *P. shikokuense* (Fig. 1). Since similar expression patterns and enriched pathways were observed when temperature changed at 19°C and 22°C relative to 25°C (Fig. 2 and S2), we focused on the changes in the DEPs and DEMs between 19°C and 25°C to reveal low temperature acclimation strategies. When photosynthetic organisms are exposed to cold stress, the photosynthetic rate decreases and excessive electrons are transferred to O_2 to generate reactive oxygen species (ROS) (50). The antioxidant enzymes and scavengers in plants and algae are normally initiated to reduce the negative effects of excess ROS on proteins, DNA, and lipids (51). The relatively low photosynthetic efficiency and highly expressed antioxidant enzymes of Cu/Zn SOD and CSPs at 19°C (Fig. 1B and 6B) may imply the excess production of ROS in *P. shikokuense* at this temperature. Alternatively, organisms can overproduce

glutathione to relieve oxidative damage caused by ROS (52). In our study, KEGG analyses of both DEPs and DEMs showed that glutathione metabolism was enriched at 19°C. The six essential enzymes glutamate-cysteine ligase catalytic subunit (GCLC), glutathione *S*-transferase (GST), glutathione dehydrogenase/transferase (DHAR), isocitrate dehydrogenase (IDH1), 6-phosphogluconate dehydrogenase (PGD), and L-ascorbate peroxidase (APX) (Fig. S3A and Table S1) and the three metabolites glutathione (GSH), glutathione disulfide, and ascorbate were significantly upregulated at 19°C compared with 25°C (Table S2), indicating their important roles in ROS scavenging at low temperature.

Since low temperature may damage the plasma membrane, phytoplankton adjust the composition of their plasma membranes to optimize the liquid/crystalline physical structure necessary for proper membrane function (53, 54). Lipids, the major component of algal plasma membrane, are made up of phospholipids, sterols and fatty acids. A series of key proteins involved in glycerophospholipid metabolism, e.g., glycerol-3-phosphate dehydrogenase (GPD1), acetylcholinesterase (ACHE), and 1-acylglycerone phosphate reductase (AYR1), and steroid biosynthesis, e.g., delta14-sterol reductase (TM7SF2), delta24-sterol reductase (DHCR24), sterol 24-C-methyltransferase (SMT1), and cycloartenol synthase (CAS1), were significantly upregulated at 19°C compared with 25°C (Fig. S3B and Table S1). Higher expressions of these enzymes reflected accumulations of glycerophospholipid and steroid in plasma membrane to cope with low temperature stress. In addition, the absolute content and relative proportion of saturated and polyunsaturated fatty acids determine the plasma membrane fluidity (55). Previous studies report sharp increases of total and polyunsaturated fatty acids in dinoflagellates during the transition from 30°C to 15°C (16) and higher proportions of polyunsaturated fatty acids in cold-adapted dinoflagellates than warm-adapted species (56). Enzymes such as fabD, FASN, ACSL, and ACSBG for fatty acid biosynthesis and enzyme ACAA1 for polyunsaturated fatty acid biosynthesis were more highly expressed at 19°C than 25°C (Fig. 6B and Fig. S4C), implying the possible greater accumulation of fatty acids in *P. shikokuense* at low temperature. Glutarate semialdehyde, a straight chain fatty acid, and 5-KETE, a long-chain fatty acid, were largely accumulated at 19°C (Fig. 6C). Since the profile of fatty acids is seldom reported in phytoplankton especially under high- or low-temperature stresses, little is known about the exact role of these fatty acids identified in low-temperature acclimation. However, it is reasonable to propose that the greater accumulation of these two fatty acids at 19°C was incorporated into the plasma membrane of *P. shikokuense* to compensate for the reduced membrane fluidity (Fig. 7).

Allocation of P and N for bloom occurrence. Spliceosome and mRNA surveillance pathway were significantly enriched at 19°C compared with 25°C (Fig. 2C). Active alternative pre-mRNA splicing, which is controlled by spliceosome, can be quickly induced to produce protein isoforms under low temperature (57, 58). Hence, the enriched spliceosome and mRNA surveillance pathway in *P. shikokuense* guaranteed the correctness of gene expression and protein synthesis at low temperature. More nucleotides at low temperature should be required as the spliceosome is mainly composed of five small nuclear RNAs (snRNAs). Consistently, the majority of DEPs and DEMs involved in purine and pyrimidine nucleotide metabolism was significantly upregulated at 19°C than 25°C (Fig. 6B and C). Enzymes such as ADK, IMPDH, and guaA, responsible for catalytic conversion of adenosine and AMP to DNA, and udk and pyrG for catalytic conversion of cytosine to RNA were observed (Fig. 7). Indeed, the omics results were supported by a decrease in the content of DNA per cell from 19°C to 25°C (Fig. 1B). The low content of RNA at high temperature was consistent with the "translation compensation hypothesis," which states that because ribosomal reaction rate increases with temperature, low ribosomal density is needed to sustain the same level of protein synthesis at high temperature (20, 59). Moreover, higher contents of DNA and RNA at 19°C than 25°C may be due to an arrest at G_2 phase of part of the *P. shikokuense* cell population, which needs further investigation. The central compositional element role played by P in nucleic acids (60) indicated that *P. shikokuense* largely allocated P to DNA and RNA at low temperature. The limited P availability in the coastal ECS is one major factor

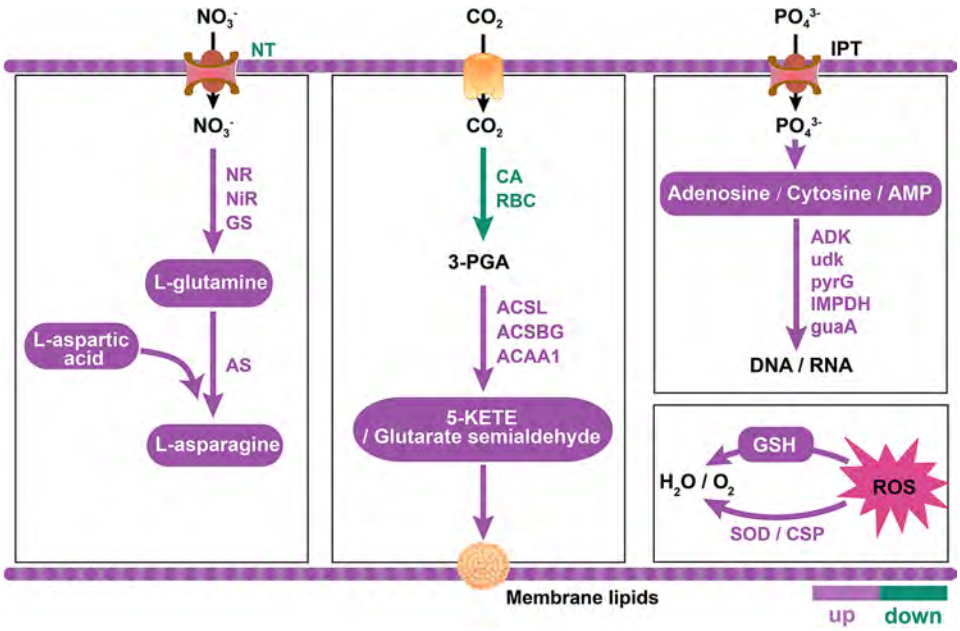

FIG 7 Schematic illustration of the key differentially expressed proteins (DEPs) and differentially expressed metabolites (DEMs) in *Prorocentrum shikokuense* involved in nutrient storage and stress acclimation at 19°C. Red and green colors represent the upregulated and downregulated levels at 19°C compared with 25°C. IPT, inorganic phosphate transporter.

regulating the bloom successions from diatom to dinoflagellate *P. shikokuense* (25). The powerful P remodeling and storage capacities, as reflected in the accelerated ATP cycling, the switch from phospholipids to nonphospholipids, and the formation of polyphosphate, are reported to largely contribute to the occurrence of *P. shikokuense* blooms (61, 62). Additionally, the high demand for P and the preferential allocation of P into DNA and RNA at 19°C indicated that a relatively large amount of P was retained in DNA and RNA at low temperature. Once seawater temperature increases, the elemental P in DNA and RNA can be remodeled into other essential compounds for cell growth, and therefore partially relieve the low P stress caused by the diatom blooms.

The strong metabolic capability of organic compounds, such as amino acids and peptides, is a competitive advantage that facilitates *P. shikokuense* bloom under low inorganic nutrient condition (63). In our study, nearly half of the differentially expressed amino acids such as GABA, L-glutamine, L-aspartic acid, and L-asparagine was found to accumulate more at 19°C rather than 25°C (Fig. 6C). Moreover, the contents of L-asparagine, L-glutamine, and GABA were included in the top 10 abundant amino acids identified at 19°C (Table S2). Accumulation of amino acids and their derivatives is a common protective mechanism for phytoplankton to relieve low temperature stress (64). The four accumulated amino acids in *P. shikokuense* at 19°C may play the same role. Indeed, greater GABA accumulation at low temperature acclimation has been reported in plants and green algae (65–67). In addition, asparagine is an ideal N storage compound that exhibits a high N:C ratio compared with other amino acids (68). It is synthesized from glutamine and aspartic acid in the ATP-dependent reaction catalyzed by the enzyme AS. AS was observed to be more (although not significantly) highly expressed at 19°C than 25°C. Moreover, NR and NiR, which catalyze the reduction of nitrate to ammonia, and GS, which further incorporates ammonia into glutamine, were more highly expressed (although not significantly) at 19°C than 25°C (Fig. 7 and Fig. S3D). The consistent expression pattern of these enzymes and metabolites suggested that cellular N flux was largely channeled into glutamine, aspartic acid, and asparagine at low temperatures. Combined with the large amount of PON per cell at 19°C (Fig. 1C), these results indicated that these amino acids may serve as important N storage pools for *P. shikokuense* under low temperature. Once the seawater temperature

increases, the stored N within them can be quickly reallocated into other necessary macromolecules (e.g., proteins and Chls) to sustain higher growth rates for bloom occurrence.

Conclusion. Our study sheds light on the response mechanisms invoked by the dinoflagellate *P. shikokuense* to sustain growth under a temperature gradient (19 to 28°C), which covers the whole bloom period from early to late spring in the coastal ECS. We observed that *P. shikokuense* exhibited increasing growth rates from 19°C to 25°C. Along this gradient, pathways of photosynthesis-antenna proteins, porphyrin and chlorophyll metabolism, photosynthesis, carbohydrate metabolism, and ribosome were consistently upregulated. Compared with 25°C, cells at 28°C endured moderate heat stress as they showed similar growth rates but a lower Fv/Fm value. Proteins involved in photoreaction, light harvesting, and protein homeostasis, such as LHP, CAB, and HSP, were more highly expressed to compensate for the negative effects of the moderate heat stress. Soluble sugars such as L-fucose, mannitol, D-mannose, sorbitol, and stachyose were largely accumulated at 28°C to compensate for the reduced carbon metabolism and sustain osmotic homeostasis. In addition, metabolites such as glutathione, glutarate semialdehyde, 5-KETE, and GABA were found, which may play important roles in low-temperature acclimation. Moreover, the significant accumulation of the nucleotides adenosine, cytosine, and AMP and the amino acids L-asparagine, L-glutamine, and L-aspartic acid at 19°C may serve as important P and N repositories that can be reallocated into other necessary macromolecules to form large-scale blooms when ocean temperature increases.

Based on the number of macromolecules detected, metabolomics showed a relatively lower identification depth than proteomics. This was mainly caused by the complex physicochemical property of metabolites and the limited phytoplankton reference database for metabolite identification. However, it is interesting to note that the two approaches were complementary and some findings could be confirmed by cross-correlations. Since abiotic factors such as temperature, nutrient, and light initially control the growth rate and cell stoichiometry of photosynthetic organisms in global oceans (20), further combined use of proteomics and metabolomics promises a better understanding of how interactions among these abiotic factors affect marine dinoflagellates. Insights gained from such studies will help us to comprehensively understand the community variation and distribution trends of marine dinoflagellates in a warming ocean.

MATERIALS AND METHODS

Microalga isolation and culture. Strain of *P. shikokuense* (CCMA206) was originally isolated from the frequent bloom-occurring coastal ECS in 2014 and was provided by the Collection Center of Marine Algae (CCMA), Xiamen University, China. Batch cultures of *P. shikokuense* were maintained in K medium (69) prepared with 0.22 μm filtered and autoclaved seawater (30 psu) and grown under cool white fluorescent light at an irradiance of 100 μmol quanta m^{-2} s^{-1} with a 14:10-h light:dark cycle at 25°C. The stock cultures were maintained at the exponential phase by dilution with fresh medium approximately every 6 days. Bactericidal penicillin (100 U/ml) and streptomycin (0.1 mg/ml) were added into the stock culture to minimize the growth of bacteria before the commencement of temperature experiments.

Experimental design. Triplicated experiments at 19, 22, 25, and 28°C were performed in 2 liters of acid-washed and autoclaved polycarbonate bottles containing 1.6 liter of medium. To obtain cells with a stable metabolic activity, *P. shikokuense* at each temperature were cultured and semicontinuously diluted daily for approximately 20 days before sampling. Cell cultures were diluted every morning with fresh medium to an initial cell density of approximately 10,000 cells/ml for a diurnal cycle. Sampling was conducted every day consecutively for 10 days.

Growth rate and thermal trait. Culture suspension (1 ml for each sample), fixed by mixing with Lugol's solution (5 μL), was counted daily before and after the dilutions with a light microscope. The growth rate was calculated using the equation: $\mu = \ln(N_2/N_1)/(t_2 - t_1)$, where N_1 is the cell density after dilution at day 1 (t_1) and N_2 is the cell density before dilution at day 2 (t_2), respectively. A unimodal extension of the Boltzmann-Arrhenius model was performed to determine the optimal growth temperature (70). We added an experiment at 30°C to increase the model accuracy. The data on growth rates at different temperatures were applied to fit the model:

$$\mu = \mu_0 \frac{e^{\frac{E_a}{k_b}\left(\frac{1}{T_0}-\frac{1}{T}\right)}}{1+\frac{E_a}{E_h-E_a}e^{\frac{E_a}{k_b}\left(\frac{1}{T_{opt}}-\frac{1}{T}\right)}},$$

where μ is the specific growth rate at each temperature, μ_0 is a preexponential constant independent of temperature, k_b is Boltzmann`s constant (8.62×10^{-5} evK^{-1}), E_a is estimated as the slope of linear regression of the log-transformed rate against the Boltzmann temperature-$1/k_bT$, T_{opt} is the optimal

temperature at which the rate reaches the maximum value, and E_h is added to describe the "steepness" of the decrease of the rate when the temperature exceeds T_{opt}.

Fv/Fm, DNA, POC, and PON measurement. To determine the maximum photochemical efficiency of PSII (Fv/Fm), whole cultures (5 ml for each sample) at 19, 22, 25, and 28°C were dark adapted for 15 min and then measured daily using a PHYTO-PAM (Walz GmbH, Effeltrich, Germany). Whole cultures (20 ml for each sample) at the four investigated temperatures were harvested by centrifugation (6,000 × *g*, 10 min, 4°C) at day 4. Cell pellets were suspended in 0.5 ml solution I (50 mM Tris-HCl, 50 mM EDTA, and 50 mM sucrose [pH 8.0]) reagent for DNA extraction. Cell pellets were frozen in liquid nitrogen for 5 min and sonicated in ice, and then DNA extractions were performed following the enzyme/phenol-chloroform extraction protocol (71). DNA concentration was quantified using the NanoDrop 2000 (Thermo Fisher Scientific, Wilmington, DE, USA).

Whole cultures (10 ml for each sample) at the four investigated temperatures were filtered through precombusted (500°C, 4 h) 1.6-μm GF/A membranes (diameter 25 mm) at day 4. The filtration membranes were exposed to HCl fumes and oven dried at 65°C for 24 h to remove inorganic carbon and nitrogen before mass spectrometric (MS) analysis. The POC and PON were determined using a PE 2400 Series II CHNS elemental analyzer (Perkin Elmer, Norwalk, CT, USA). Statistical comparisons of the treatment groups were assessed with one-way ANOVA using SPSS22.0 software (SPSS Inc., Chicago, IL, USA).

Protein extraction, digestion, peptide labeling, and liquid chromatography-MS/MS analysis. Whole cultures (100 ml for each sample) at 19, 22, 25, and 28°C were harvested by centrifugation (6,000 × *g*, 10 min, 4°C) at day 4. The pelleted cells were immediately frozen in liquid nitrogen and then stored at −80°C before further processing. Cell pellets (of two of the three biological repeats for each temperature) were suspended in 1 ml TRIzol (Invitrogen, Carlsbad, CA, USA) reagent for protein extraction, following the previous protocol (72). Protein concentration was quantified using a 2D Quant kit (GE Healthcare, San Francisco, CA, USA). After adjusting the pH to 8.5 with 1 M ammonium bicarbonate, 100 μg protein from each sample was first reduced with DTT (1 h) at 60°C and then alkylated with iodoacetamide (45 min, in the dark) at room temperature. Each sample was digested twice using Trypsin Gold (Promega, Madison, WI, USA) with a protein/trypsin ratio of 30:1 (wt/wt) for 14 h at 37°C. After desalting on a Strata X C18 solid-phase extraction column (Phenomenex, Torrance, CA, USA), trypsin-digested samples were evaporated and reconstituted in 0.2 M triethylammonium bicarbonate (TEAB). Desalted peptides of eight samples (two biological repeats for each temperature) were then labeled with iTRAQ reagents 8-plex kit (Applied Biosystems, Foster City, CA, USA) according to the manufacturer's instructions: Tag113 and Tag114, 19°C; Tag115 and Tag116, 22°C; Tag117 and Tag118, 25°C; and Tag119 and Tag121, 28°C. After a 2 h of incubation, the labeled samples were combined, desalted with a Strata X C18 column (Phenomenex), and then vacuum dried.

The peptides were reconstituted with buffer A (5% ACN, pH adjusted to 9.8 with ammonia) to 2 ml and then were separated on a Shimadzu LC-20AB HPLC Pump system coupled with a high-pH RP column. The peptides were separated at a flow rate of 1 ml/min with isocratic 5% buffer B (95% ACN, pH 9.8) for 10 min, a gradient from 5% to 35% buffer B over 40 min, then 35% to 95% buffer B over 1 min. The system was then maintained at 95% buffer B for 3 min before being decreased to 5% within 1 min, and the column was reequilibrated with 5% buffer B for 10 min. A total of 20 fractions were collected and vacuum dried.

Each fraction was resuspended in buffer C (2% ACN and 0.1% FA) and centrifuged at 16,000 × *g* for 10 min. The supernatant was loaded onto a C18 trap column 5 μL/min for 8 min using a LC-20AD nano-HPLC instrument (Shimadzu, Kyoto, Japan) autosampler that was interfaced to a Q EXACTIVE mass spectrometer (Thermo Fisher Scientific, San Jose, CA, USA). The peptides were eluted from the trap column and separated by a capillary C18 column (inner diameter, 75 μm) packed in-house. The gradient was run at 300 nl/min starting from 8% to 35% of buffer D (98% ACN and 0.1% FA) in 35 min, then going up to 60% in 5 min, then maintained at 80% D for 5 min, and finally returned to 5% in 0.1 min and equilibrated for 10 min. The separated peptides were subject to nano-electrospray ionization (nano-ESI) and MS data-dependent acquisition (DDA). The parameters for MS analysis were as follows: electrospray voltage, 1.6 kV; precursor scan range, 350 to 1,600 *m/z* at a resolution of 70,000 in Orbitrap; MS/MS fragment scan range, >100 *m/z* at a resolution of 175,000 in HCD mode; normalized collision energy setting, 27%; dynamic exclusion time, 15 s; and automatic gain control (AGC) for full MS target and MS2 target, 3e6 and 1e5, respectively; The number of MS/MS scans following 1 MS scan was 20 most abundant precursor ions above a threshold ion count of 20,000.

Protein identification, quantification, and bioinformatics analysis. The raw MS/MS data were converted to MGF files by Proteome Discoverer 1.4 (Thermo Scientific, Waltham, MA, USA) and the exported MGF files were searched using Mascot (v2.3.02, MatrixScience; London, UK) against a database containing translated protein sequences from transcriptomes of *P. shikokuense* pure culture (73). Mascot parameters were set as follows: trypsin was selected as the specific enzyme with a maximum of two missed cleavages permitted per peptide; fixed modifications of carbamidomethyl (C), iTRAQ8-plex (N-term), and iTRAQ8-plex (K); variable modifications consisting of oxidation (M); peptide charge, 2+, 3+, and 4+; 20 ppm of peptide mass tolerance; and 0.05 Da of fragment mass tolerance. The automatic Mascot decoy database search was performed. The Mascot results were processed by IQuant utilizing MascotPercolator to rescore the peptide spectrum matches (PSMs) (74). The identified peptide sequences were assembled into a set of confident proteins using the Occam's razor approach implemented in IQuant, and the false discovery rate (FDR) at 1% was set in both PSM and protein levels. For this study, high-confidence proteins containing at least one unique peptide and two unique spectra were chosen and DEPs (differentially expressed proteins) were filtered with the cutoffs of fold ratios ≥1.2 or ≤0.83 and *P* value of <0.05. Functional annotations were performed against the database of NCBI

nonredundant protein (NCBInr) and Kyoto Encyclopedia of Genes and Genomes (KEGG), and KEGG enrichment of DEPs was performed using the R package GSEA.

Metabolite extraction and LC-ESI/MS analysis. Biological activity of the cultured *P. shikokuense* cells (100 ml for each sample) was first quenched by adding 50 μL $HgCl_2$ saturated solution. Whole cultures at 19, 25, and 28°C were harvested by centrifugation (6,000 g, 10 min, 4°C) at day 4, immediately frozen in liquid nitrogen and then stored at −80°C. Cell pellets (6 repeats for each temperature) were suspended in 2 ml centrifuge tube with 1 ml extraction buffer (acetonitrile:methanol:water, 2:2:1, vol/vol/vol) and 100-mg glass beads. The centrifuge tubes were allowed to freeze in liquid nitrogen for 5 min and then thawed at room temperature. The thawed samples were then ground at 55 Hz for 2 min (the freeze-thaw-grind cycle was repeated 3 times). Following another round of centrifugation (12,000 × *g*, 10 min, 4°C), the supernatant was transferred to a new tube, vacuum-dried and redissolved in 300 μL 2-amino-3-(2-chloro-phenyl)-propionic acid (4 ppm). The solution was then filtered through a 0.2 μm (PALL Life Sciences, USA) membrane prior to LC-MS/MS analysis.

LC-MS/MS analysis was conducted on a Vanquish UHPLC System (Thermo Fisher Scientific, USA) using an ACQUITY UPLC HSS T3 (150 × 2.1 mm, 1.8 μm) (Waters, Milford, MA, USA). The column was maintained at 40°C. The flow rate and injection volume were set at 250 μL/min and 2 μL, respectively. For LC-ESI (+)/MS analysis, the mobile phases consisted of buffer E (0.1% formic acid in CAN) and buffer F (0.1% formic acid in water). Separation was conducted under the following gradient: 2% E, 0 to 1 min; 2 to 50% E, 1 to 9 min; 50 to 98% E, 9 to 12 min; 98% E, 12 to 13.5 min; 98 to 2% E, 13.5 to 14 min; and 2% E, 14 to 20 min. For LC-ESI(−)/MS analysis, the analysis was carried out with mobile phases of ACN and ammonium formate (5 mM). Separation was conducted under the following gradient: 2% ACN, 0 to 1 min; 2 to 50% ACN, 1 to 9 min; 50 to 98% ACN, 9 to 12 min; 98% ACN, 12 to 13.5 min; 98% to 2% ACN, 13.5 to 14 min; and 2% ACN, 14 to 17 min.

Mass spectrometric detection of metabolites was performed on Q Exactive (Thermo Fisher Scientific, USA) with ESI ion source. Simultaneous MS1 and MS/MS (full MS-ddMS2 mode, data-dependent MS/MS) acquisition was used. The parameters were as follows: sheath gas pressure, 30 arb; aux gas flow, 10 arb; spray voltage, 3.50 kV and −2.50 kV for ESI(+) and ESI(−), respectively; capillary temperature, 325°C; MS1 range, *m/z* 81 to 1,000; MS1 resolving power, 70,000 FWHM; number of data dependent scans per cycle, 10; MS/MS resolving power, 17,500 FWHM; normalized collision energy, 30%; and dynamic exclusion time, automatic.

Metabolite identification, quantification, and bioinformatics analysis. The raw data were converted to mzXML format by MSConvert in the ProteoWizard software package (v3.0.8789) (75) and processed using XCMS for feature detection, retention time correction and alignment. The metabolites were identified by mass accuracy (<30 ppm) and MS/MS data that were matched with HMDB, Massbank, LipidMaps, mzclound, and KEGG. The robust LOESS signal correction (QC-RLSC) was applied for data normalization to correct for any systematic bias. After normalization, only ion peaks with relative standard deviations (RSDs) less than 30% in QC were kept to ensure proper metabolite identification.

All the multivariate data analyses were performed using Ropls software (76). After scaling data, models were built on principal-component analysis, orthogonal partial least-square discriminant analysis (PLS-DA) and partial least-square discriminant analysis (OPLS-DA). The metabolite profiles were visualized as score plot with each point representing a sample. The corresponding loading plot and S-plot were generated to provide information on the metabolites that influence clustering of the samples. All the models evaluated were tested for over fitting with methods of permutation tests. The descriptive performance of the models was determined by R2X (cumulative) (perfect model: R2X [cum] = 1) and R2Y (cumulative) (perfect model: R2Y [cum] = 1) values while their prediction performance was measured by Q2 (cumulative) (perfect model: Q2 [cum] = 1) and a permutation test. The permuted model was applied to predict classes: R2 and Q2 values at the *y* axis intercept must be lower than those of Q2 and the R2 of the nonpermuted model. OPLS-DA allowed the determination of discriminating metabolites using the variable importance on projection (VIP). The *P* value, VIP and fold change (FC) were applied to discover the contributable-variable for classification. Finally, a *P* value of <0.05 and VIP values of >1 were considered to be statistically differentially expressed metabolites (DEMs). The identified metabolites were functionally annotated to the KEGG database, and pathway enrichment and topology analyses of DEMs were performed using MetaboAnalyst (77).

Data availability. The mass spectrometry proteomics data were deposited to the ProteomeXchange Consortium via the PRIDE partner repository with the data set identifier PXD033681.

SUPPLEMENTAL MATERIAL

Supplemental material is available online only.

SUPPLEMENTAL FILE 1, XLSX file, 2.8 MB.

SUPPLEMENTAL FILE 2, XLSX file, 0.2 MB.

SUPPLEMENTAL FILE 3, PDF file, 0.7 MB.

ACKNOWLEDGMENTS

This work was supported by National Natural Science Foundation of China (NSFC) grants 42076155 and 41606132, China Postdoctoral Science Foundation grants 2019M663152 and 2020T130662 (to H.Z.), Key Special Project for Introduced Talents Team of Southern Marine Science and Engineering Guangdong Laboratory (Guangzhou) grant GML2019ZD0405, and

CAS Pioneer Hundred Talents Program grants Y8SL031001 and Y9YB021001 (to X.X.). Y.Z. and Z.X. acknowledge the financial support from NSFC grant 41973072 (to Y.Z.) and grant 41906087 (to Z.X.).

We thank C. H. Hocart for improving the English of this manuscript. This is contribution no. 2x from the Isotopomics in Chemical Biology (ICB) group.

We declare no competing interests.

REFERENCES

1. Ibarbalz FM, Henry N, Brandão MC, Martini S, Busseni G, Byrne H, Coelho LP, Endo H, Gasol JM, Gregory AC, Mahé F, Rigonato J, Royo-Llonch M, Salazar G, Sanz-Sáez I, Scalco E, Soviadan D, Zayed AA, Zingone A, Labadie K, Ferland J, Marec C, Kandels S, Picheral M, Dimier C, Poulain J, Pisarev S, Carmichael M, Pesant S, Acinas SG, Babin M, Bork P, Boss E, Bowler C, Cochrane G, de Vargas C, Follows M, Gorsky G, Grimsley N, Guidi L, Hingamp P, Iudicone D, Jaillon O, Kandels S, Karp-Boss L, Karsenti E, Not F, Ogata H, Pesant S, Poulton N, Tara Oceans Coordinators, et al. 2019. Global trends in marine plankton diversity across kingdoms of life. Cell 179:1084–1097. https://doi.org/10.1016/j.cell.2019.10.008.
2. Righetti D, Vogt M, Gruber N, Psomas A, Zimmermann NE. 2019. Global pattern of phytoplankton diversity driven by temperature and environmental variability. Sci Adv 5:eaau6253. https://doi.org/10.1126/sciadv.aau6253.
3. Li G, Cheng L, Zhu J, Trenberth KE, Mann ME, Abraham JP. 2020. Increasing ocean stratification over the past half-century. Nat Clim Chang 10:1116–1123. https://doi.org/10.1038/s41558-020-00918-2.
4. Thomas MK, Kremer CT, Klausmeier CA, Litchman E. 2012. A global pattern of thermal adaptation in marine phytoplankton. Science 338:1085–1088. https://doi.org/10.1126/science.1224836.
5. Anderson DM, Alpermann TJ, Cembella AD, Collos Y, Masseret E, Montresor M. 2012. The globally distributed genus Alexandrium: multifaceted roles in marine ecosystems and impacts on human health. Harmful Algae 14:10–35. https://doi.org/10.1016/j.hal.2011.10.012.
6. Brand LE, Campbell L, Bresnan E. 2012. Karenia: the biology and ecology of a toxic genus. Harmful Algae 14:156–178. https://doi.org/10.1016/j.hal.2011.10.020.
7. Gobler CJ, Doherty OM, Hattenrath-Lehmann TK, Griffith AW, Kang Y, Litaker RW. 2017. Ocean warming since 1982 has expanded the niche of toxic algal blooms in the North Atlantic and North Pacific oceans. Proc Natl Acad Sci U S A 114:4975–4980. https://doi.org/10.1073/pnas.1619575114.
8. Xiao W, Liu X, Irwin AJ, Laws EA, Wang L, Chen B, Zeng Y, Huang B. 2018. Warming and eutrophication combine to restructure diatoms and dinoflagellates. Water Res 128:206–2285. https://doi.org/10.1016/j.watres.2017.10.051.
9. Anderson SI, Barton AD, Clayton S, Dutkiewicz S, Rynearson TA. 2021. Marine phytoplankton functional types exhibit diverse responses to thermal change. Nat Commun 12:6413. https://doi.org/10.1038/s41467-021-26651-8.
10. Ras M, Steyer J-P, Bernard O. 2013. Temperature effect on microalgae: a crucial factor for outdoor production. Rev Environ Sci Biotechnol 12:153–164. https://doi.org/10.1007/s11157-013-9310-6.
11. Sparrow L, Momigliano P, Russ GR, Heimann K. 2017. Effects of temperature, salinity and composition of the dinoflagellate assemblage on the growth of Gambierdiscus carpenteri isolated from the Great Barrier Reef. Harmful Algae 65:52–60. https://doi.org/10.1016/j.hal.2017.04.006.
12. Jeong HJ, Lee KH, Yoo YD, Kang NS, Song JY, Kim TH, Seong KA, Kim JS, Potvin E. 2018. Effects of light intensity, temperature, and salinity on the growth and ingestion rates of the red-tide mixotrophic dinoflagellate Paragymnodinium shiwhaense. Harmful Algae 80:46–54. https://doi.org/10.1016/j.hal.2018.09.005.
13. Iglesias-Prieto R, Matta JL, Robins WA, Trench RK. 1992. Photosynthetic response to elevated temperature in the symbiotic dinoflagellate Symbiodinium microadriaticum in culture. Proc Natl Acad Sci U S A 89:10302–10305. https://doi.org/10.1073/pnas.89.21.10302.
14. Lomas MW, Glibert PM. 1999. Temperature regulation of nitrate uptake: a novel hypothesis about nitrate uptake and reduction in cool water diatoms. Limnol Oceanogr 44:556–572. https://doi.org/10.4319/lo.1999.44.3.0556.
15. Barati B, Gan SY, Lim PE, Beardall J, Phang SM. 2019. Green algal molecular responses to temperature stress. Acta Physiol Plant 41:348. https://doi.org/10.1007/s11738-019-2813-1.
16. Hyun B, Ju SJ, Ko AR, Choi KH, Jung SW, Jang PG, Jang MC, Moon C, Shin K. 2016. Thermal effects on the growth and fatty acid composition of four harmful algal bloom species: possible implications for ichthyotoxicity. Ocean Sci J 51:333–342. https://doi.org/10.1007/s12601-016-0029-5.
17. Navarro J, Muñoz MG, Contreras A. 2006. Temperature as a factor regulating growth and toxin content in the dinoflagellate Alexandrium catenella. Harmful Algae 5:762–769. https://doi.org/10.1016/j.hal.2006.04.001.
18. Granéli E, Vidyarathna NK, Funari E, Cumaranatunga PRT, Scenati R. 2011. Can increases in temperature stimulate blooms of the toxic benthic dinoflagellate Ostreopsis ovata. Harmful Algae 10:165–172. https://doi.org/10.1016/j.hal.2010.09.002.
19. Aguilera-Belmonte A, Inostroza I, Carrillo KS, Franco JM, Riobó P, Gómez PI. 2013. The combined effect of salinity and temperature on the growth and toxin content of four Chilean strains of Alexandrium catenella (Whedon and Kofoid) Balech 1985 (Dinophyceae) isolated from an outbreak occurring in southern Chile in 2009. Harmful Algae 23: 55–59. https://doi.org/10.1016/j.hal.2012.12.006.
20. Toseland A, Daines SJ, Clark JR, Kirkham A, Strauss J, Uhlig C, Lenton TM, Valentin K, Pearson GA, Moulton V, Mock T. 2013. The impact of temperature on marine phytoplankton resource allocation and metabolism. Nat Clim Chang 3:979–984. https://doi.org/10.1038/nclimate1989.
21. Shin H, Hong S-J, Yoo C, Han M-A, Lee H, Choi H-K, Cho S, Lee C-G, Cho B-K. 2016. Genome-wide transcriptome analysis revealed organelle specific responses to temperature variations in algae. Sci Rep 6:37770. https://doi.org/10.1038/srep37770.
22. Liang Y, Koester JA, Liefer JD, Irwin AJ, Finkel ZV. 2019. Molecular mechanisms of temperature acclimation and adaptation in marine diatoms. ISME J 13:2415–2425. https://doi.org/10.1038/s41396-019-0441-9.
23. Kobiyama A, Tanaka S, Kaneko Y, Lim PT, Ogata T. 2010. Temperature tolerance and expression of heat shock protein 70 in the toxic dinoflagellate Alexandrium tamarense (Dinophyceae). Harmful Algae 9:180–185. https://doi.org/10.1016/j.hal.2009.09.002.
24. Rosic NN, Pernice M, Dove S, Dunn S, Hoegh-Guldberg O. 2011. Gene expression profiles of cytosolic heat shock proteins Hsp70 and Hsp90 from symbiotic dinoflagellates in response to thermal stress: possible implications for coral bleaching. Cell Stress Chaperones 16:69–80. https://doi.org/10.1007/s12192-010-0222-x.
25. Lu S, Ou L, Dai X, Cui L, Dong Y, Wang P, Li D, Lu D. 2022. An overview of Prorocentrum donghaiense blooms in China: species identification, occurrences, ecological consequences, and factors regulating prevalence. Harmful Algae 114:102207. https://doi.org/10.1016/j.hal.2022.102207.
26. GÓMEZ F, Zhang H, Roselli L, Lin SJ. 2022. Detection of *Prorocentrum shikokuense* in the Mediterranean Sea and evidence that *P dentatum*, *P obtusidens* and *P shikokuense* are three different species (Prorocentrales, Dinophyceae). Acta Protozool 60:47–59. https://doi.org/10.4467/16890027AP.21.006.15380.
27. Li Y, Lü S, Jiang T, Xiao Y, You S. 2011. Environmental factors and seasonal dynamics of Prorocentrum populations in Nanji Islands National Nature Reserve, East China Sea. Harmful Algae 10:426–432. https://doi.org/10.1016/j.hal.2010.08.002.
28. Xu N, Duan S, Li A, Zhang C, Cai Z, Hu Z. 2010. Effects of temperature, salinity and irradiance on the growth of the harmful dinoflagellate Prorocentrum donghaiense Lu. Harmful Algae 9:13–17. https://doi.org/10.1016/j.hal.2009.06.002.
29. Geider R, La Roche J. 2002. Redfield revisited: variability of C:N:P in marine microalgae and its biochemical basis. Eur J Phycol 37:1–17. https://doi.org/10.1017/S0967026201003456.
30. Falkowski PG. 2000. Rationalizing elemental ratios in unicellular algae. J Phycol 36:3–6. https://doi.org/10.1046/j.1529-8817.2000.99161.x.
31. Montagnes DJS, Franklin M. 2001. Effect of temperature on diatom volume, growth rate, and carbon and nitrogen content: reconsidering some paradigms. Limnol Oceanogr 46:2008–2018. https://doi.org/10.4319/lo.2001.46.8.2008.

32. Garcia N, Sexton J, Riggins T, Brown J, Lomas M, Martiny A. 2018. High variability in cellular stoichiometry of carbon, nitrogen, and phosphorus within classes of marine eukaryotic phytoplankton under sufficient nutrient conditions. Front Microbiol 9:543. https://doi.org/10.3389/fmicb.2018.00543.
33. Atkinson D. 1994. Temperature and organism size–a biological law for ectotherms? Adv Ecol Res 25:1–58. https://doi.org/10.1016/S0065-2504(08)60212-3.
34. O'Donnell DR, Beery SM, Litchman E. 2021. Temperature-dependent evolution of cell morphology and carbon and nutrient content in a marine diatom. Limnol Oceanogr 66:4334–4346. https://doi.org/10.1002/lno.11964.
35. Vidal-Melgosa S, Sichert A, Francis TB, Bartosik D, Niggemann J, Wichels A, Willats WGT, Fuchs BM, Teeling H, Becher D, Schweder T, Amann R, Hehemann J-H. 2021. Diatom fucan polysaccharide precipitates carbon during algal blooms. Nat Commun 12:1150–1150. https://doi.org/10.1038/s41467-021-21009-6.
36. Tonon T, Li Y, McQueen-Mason S. 2017. Mannitol biosynthesis in algae: more widespread and diverse than previously thought. New Phytol 213: 1573–1579. https://doi.org/10.1111/nph.14358.
37. Adams JMM, Ross AB, Anastasakis K, Hodgson EM, Gallagher JA, Jones JM, Donnison IS. 2011. Seasonal variation in the chemical composition of the bioenergy feedstock Laminaria digitata for thermochemical conversion. Bioresour Technol 102:226–234. https://doi.org/10.1016/j.biortech.2010.06.152.
38. Moore CM, Suggett DJ, Hickman AE, Kim Y-N, Tweddle JF, Sharples J, Geider RJ, Holligan PM. 2006. Phytoplankton photoacclimation and photoadaptation in response to environmental gradients in a shelf sea. Limnol Oceanogr 51:936–949. https://doi.org/10.4319/lo.2006.51.2.0936.
39. Nishiyama Y, Murata N. 2014. Revised scheme for the mechanism of photoinhibition and its application to enhance the abiotic stress tolerance of the photosynthetic machinery. Appl Microbiol Biotechnol 98:8777–8796. https://doi.org/10.1007/s00253-014-6020-0.
40. Grossman AR, Bhaya D, Fau - Apt KE, Apt Ke Fau - Kehoe DM, Kehoe DM. 1995. Light-harvesting complexes in oxygenic photosynthesis: diversity, control, and evolution. Annu Rev Genet 29:231–288. https://doi.org/10.1146/annurev.ge.29.120195.001311.
41. Peers G, Truong TB, Ostendorf E, Busch A, Elrad D, Grossman AR, Hippler M, Niyogi KK. 2009. An ancient light-harvesting protein is critical for the regulation of algal photosynthesis. Nature 462:518–521. https://doi.org/10.1038/nature08587.
42. Dittami SM, Michel G, Collén J, Boyen C, Tonon T. 2010. Chlorophyll-binding proteins revisited - a multigenic family of light-harvesting and stress proteins from a brown algal perspective. BMC Evol Biol 10:365. https://doi.org/10.1186/1471-2148-10-365.
43. Young J, Moarefi I, Hartl FU. 2001. Hsp90: a specialized but essential protein-folding tool. J Cell Biol 154:267–273. https://doi.org/10.1083/jcb.200104079.
44. Park CJ, Seo YS. 2015. Heat shock proteins: a review of the molecular chaperones for plant immunity. Plant Pathol J 31:323–333. https://doi.org/10.5423/PPJ.RW.08.2015.0150.
45. Guo R, Ebenezer V, Ki JS. 2012. Transcriptional responses of heat shock protein 70 (Hsp70) to thermal, bisphenol A, and copper stresses in the dinoflagellate Prorocentrum minimum. Chemosphere 89:512–520. https://doi.org/10.1016/j.chemosphere.2012.05.014.
46. Yokthongwattana K, Chrost B, Behrman S, Casper-Lindley C, Melis A. 2001. Photosystem II damage and repair cycle in the green alga Dunaliella salina: involvement of a chloroplast-localized HSP70. Plant Cell Physiol 42:1389–1397. https://doi.org/10.1093/pcp/pce179.
47. Hayat S, Hayat Q, Alyemeni MN, Wani AS, Pichtel J, Ahmad A. 2012. Role of proline under changing environments: a review. Plant Signal Behav 7: 1456–1466. https://doi.org/10.4161/psb.21949.
48. Bita CE, Gerats T. 2013. Plant tolerance to high temperature in a changing environment: scientific fundamentals and production of heat stress-tolerant crops. Front Plant Sci 4:273. https://doi.org/10.3389/fpls.2013.00273.
49. Ruan YL, Jin Y, Yang YJ, Li GJ, Boyer JS. 2010. Sugar input, metabolism, and signaling mediated by invertase: roles in development, yield potential, and response to drought and heat. Mol Plant 3:942–955. https://doi.org/10.1093/mp/ssq044.
50. Mittler R. 2002. Oxidative stress, antioxidants and stress tolerance. Trends Plant Sci 7:405–410. https://doi.org/10.1016/S1360-1385(02)02312-9.
51. Sharma P, Jha A, Dubey R, Pessarakli M. 2012. Reactive oxygen species, oxidative damage, and antioxidative defense mechanism in plants under stressful conditions. J Botany 2012:1–26. https://doi.org/10.1155/2012/217037.
52. Ribas V, García-Ruiz C, Fernández-Checa JC. 2014. Glutathione and mitochondria. Front Pharmacol 5:1–19. https://doi.org/10.3389/fphar.2014.00151.
53. Uemura M, Tominaga Y, Nakagawara C, Shigematsu S, Minami A, Kawamura Y. 2006. Responses of the plasma membrane to low temperatures. Physiol Plant 126:81–89. https://doi.org/10.1111/j.1399-3054.2005.00594.x.
54. Bajerski F, Wagner D, Mangelsdorf K. 2017. Cell membrane fatty acid composition of Chryseobacterium frigidisoli PB4T, Isolated from Antarctic Glacier forefield soils, in response to changing temperature and pH conditions. Front Microbiol 8:677. https://doi.org/10.3389/fmicb.2017.00677.
55. Willette S, Gill SS, Dungan B, Schaub TM, Jarvis JM, St Hilaire R, Omar Holguin F. 2018. Alterations in lipidome and metabolome profiles of Nannochloropsis salina in response to reduced culture temperature during sinusoidal temperature and light. Algal Res 32:79–92. https://doi.org/10.1016/j.algal.2018.03.001.
56. Leblond J, Anderson B, Kofink D, Logares R, Rengefors K, Kremp A. 2006. Fatty acid and sterol composition of two evolutionary closely related dinoflagellate morphospecies from cold Scandinavian brackish and freshwaters. European J Phycology 41:303–311. https://doi.org/10.1080/09670260600804843.
57. Valledor L, Furuhashi T, Hanak A-M, Weckwerth W. 2013. Systemic cold stress adaptation of Chlamydomonas reinhardtii. Mol Cell Proteomics 12: 2032–2047. https://doi.org/10.1074/mcp.M112.026765.
58. John S, Olas JJ, Mueller-Roeber B. 2021. Regulation of alternative splicing in response to temperature variation in plants. J Exp Bot 72:6150–6163. https://doi.org/10.1093/jxb/erab232.
59. Daines SJ, Clark JR, Lenton TM. 2014. Multiple environmental controls on phytoplankton growth strategies determine adaptive responses of the N:P ratio. Ecol Lett 17:414–425. https://doi.org/10.1111/ele.12239.
60. Warner JR. 1999. The economics of ribosome biosynthesis in yeast. Trends Biochem Sci 24:437–440. https://doi.org/10.1016/S0968-0004(99)01460-7.
61. Shi X, Lin X, Li L, Li M, Palenik B, Lin S. 2017. Transcriptomic and microRNAomic profiling reveals multi-faceted mechanisms to cope with phosphate stress in a dinoflagellate. ISME J 11:2209–2218. https://doi.org/10.1038/ismej.2017.81.
62. Lin S, Litaker RW, Sunda WG. 2016. Phosphorus physiological ecology and molecular mechanisms in marine phytoplankton. J Phycol 52:10–36. https://doi.org/10.1111/jpy.12365.
63. Zhang H, Xu HK, Zhang SF, Zhou Y, He YB, Amin SA, Chen JW, Yan KQ, Lin L, Liu SQ, Wang DZ. 2021. Metaproteomics reveals the molecular mechanism underlying bloom maintenance of a marine dinoflagellate under low ambient CO_2 and inorganic nutrients. Sci Total Environ 768:144515. https://doi.org/10.1016/j.scitotenv.2020.144515.
64. Ermilova E. 2020. Cold stress response: an overview in Chlamydomonas. Front Plant Sci 11:569437. https://doi.org/10.3389/fpls.2020.569437.
65. Kinnersley AM, Turano FJ. 2000. Gamma aminobutyric acid (GABA) and plant responses to stress. Crit Rev Plant Sci 19:479–509. https://doi.org/10.1080/07352680091139277.
66. Sadowsky A, Mettler-Altmann T, Ott S. 2016. Metabolic response to desiccation stress in strains of green algal photobionts (Trebouxia) from two Antarctic lichens of southern habitats. Phycologia 55:703–714. https://doi.org/10.2216/15-127.1.
67. Calhoun S, Bell TAS, Dahlin LR, Kunde Y, LaButti K, Louie KB, Kuftin A, Treen D, Dilworth D, Mihaltcheva S, Daum C, Bowen BP, Northen TR, Guarnieri MT, Starkenburg SR, Grigoriev IV. 2021. A multi-omic characterization of temperature stress in a halotolerant Scenedesmus strain for algal biotechnology. Commun Biol 4:333. https://doi.org/10.1038/s42003-021-01859-y.
68. Lea PJ, Sodek L, Parry MAJ, Shewry PR, Halford NG. 2007. Asparagine in plants. Ann Appl Biol 150:1–26. https://doi.org/10.1111/j.1744-7348.2006.00104.x.
69. Keller MD, Selvin RC, Claus W, Guillard RRL. 2007. Media for the culture of oceanic ultraphytoplankton. J Phycology 23:633–638. https://doi.org/10.1111/j.1529-8817.1987.tb04217.x.
70. Chen B, Laws EA. 2017. Is there a difference of temperature sensitivity between marine phytoplankton and heterotrophs? Limnol Oceanogr 62: 806−817. https://doi.org/10.1002/lno.10462.
71. Xia X, Leung S, Cheung S, Zhang S, Liu H. 2020. Rare bacteria in seawater are dominant in the bacterial assemblage associated with the bloom-forming dinoflagellate *Noctiluca scintillans*. Sci Total Environ 711:135107. https://doi.org/10.1016/j.scitotenv.2019.135107.
72. Wang DZ, Zhang YJ, Zhang SF, Zhang SF, Lin L, Hong HS. 2013. Quantitative proteomic analysis of cell cycle of the dinoflagellate Prorocentrum donghaiense (Dinophyceae). PLoS One 8:e63659. https://doi.org/10.1371/journal.pone.0063659.
73. Zhang SF, Yuan CJ, Chen Y, Lin L, Wang DZ. 2019. Transcriptomic response to changing ambient phosphorus in the marine dinoflagellate *Prorocentrum donghaiense*. Sci Total Environ 692:1037–1047. https://doi.org/10.1016/j.scitotenv.2019.07.291.
74. Wen B, Zhou R, Feng Q, Wang QH, Wang J, Liu SQ. 2014. IQuant: an automated pipeline for quantitative proteomics based upon isobaric tags. Proteomics 14:2280–2285. https://doi.org/10.1002/pmic.201300361.

75. Smith CA, Want EJ, O'Maille G, Abagyan R, Siuzdak G. 2006. XCMS: Processing mass spectrometry data for metabolite profiling using nonlinear peak alignment, matching, and identification. Anal Chem 78:779–787. https://doi.org/10.1021/ac051437y.
76. Thévenot E, Roux A, Xu Y, Ezan E, Junot C. 2015. Analysis of the human adult urinary metabolome variations with age, body mass index, and gender by implementing a comprehensive workflow for univariate and OPLS statistical analyses. J Proteome Res 14:3322–3335. https://doi.org/10.1021/acs.jproteome.5b00354.
77. Xia J, Wishart D. 2011. Web-based inference of biological patterns, functions and pathways from metabolomic data using MetaboAnalyst. Nat Protoc 6:743–760. https://doi.org/10.1038/nprot.2011.319.